A look into uncertainty in structural seismic performance arising from additional Rayleigh damping in inelastic time history analysis

Pierre Jehel

A look into uncertainty in structural seismic performance arising from additional Rayleigh damping in inelastic time history analysis

P. Jehel
Laboratoire MSSMat - CNRS UMR 8579, École Centrale Paris, France
Department of Civil Engineering and Engineering Mechanics, Columbia University, New York, USA

ABSTRACT: Estimating the vulnerability of a structure subjected to a certain hazard, that is the probability that it would not meet a given performance objective for a given hazardous event, is a key step in an overall seismic risk management process. Structural performance indicators, coupled to hazard analysis, directly provide decision-makers with readable information: *e.g.* the risk for a structure to collapse within a certain number of years. This work focuses on the vulnerability assessment of reinforced concrete moment-resisting frame structures subjected to seismic hazard, based on inelastic time history structural analyses. Structural analyses entail numerous uncertainties that can compromise the reliability of its outcomes and, in turn, the assessment of the structural performance. The aim of this paper is to provide insight into the uncertainty in the structural seismic performance analysis that arises from the addition of viscous damping in the inelastic time history analyses and to compare it to the variability that comes from the ground motion. Latin hypercube samples of random variables are generated and the uncertainty is propagated to the outcomes of interest using Monte Carlo simulations.

1 INTRODUCTION

1.1 *Background*

In seismic performance-based design, engineering demand parameters (EDP) are computed for a set of ground motions and of structural models sometimes too, and then expressed in terms of performance criteria which can be easily interpreted by decision-makers or other stakeholders. The concept of structural fragility, *viz.* the probability that a performance criterium will not be met for a given loading, is also useful for structural performance assessment (Tantala et al. 2008). The reliability of a performance analysis depends on the uncertainty in the EDPs, and thus on the uncertainty in the variables involved in the structural analyses. Hwang and Huo (1994) build seismic fragility curves of buildings accounting for several sources of uncertainty in the earthquake-site-structure system, among which the Rayleigh viscous damping ratio. The relative impact of each uncertainty source on the fragility curves is not discussed. Yet, estimating the sensitivity of the EDPs to the uncertain variables is particularly useful to identify which of them should be focused on to effectively reduce the overall uncertainty in the performance assessment.

Therefore, more recent studies have been dedicated to the analysis of the sensitivity of the EDPs to several uncertain variables pertaining to both the ground motion and the structural model. Porter et al. (2002) present a simple methodology to evaluate the relative contribution of each variable to the overall performance uncertainty based on assembly-based vulnerability studies. What the authors call “pure” – also referred to as “intrinsic” – damping, that is damping not generated by hysteretic energy dissipation, is one of the uncertain variables. According to experimental data corrected to eliminate the effects of hysteretic damping in the measures, a coefficient of variation (COV) of the damping ratio is expected to be around 0.3 to 0.4. Then in the structural model, Rayleigh damping is used with uncertain critical damping ratio described by a Gaussian distribution centered at 5% and with a COV of 0.4 (there is no mention of whether the damping matrix is built from the initial or the tangent stiffness). It is finally concluded, for the high-rise nonductile reinforced concrete moment-resisting frame building considered, that the most important contributions to the overall uncertainty in the model performance outputs are the fragility of the building components and the ground motion characteristics, whereas the contribution of viscous damping is shown to be significant too.

There are other studies of the sensitivity of performance outputs to structural and ground motion parameters: with focus on local output such as curvature Lee and Mosalam (2005) or on collapse assess-

ment (Liel et al. 2009), in the context of incremental dynamic analysis (Vamvatsikos and Fragiadakis 2010), where different methods for propagating the uncertainties are investigated (FOSM, Monte Carlo simulation), and where damping is sometimes considered as a source of uncertainty. Those papers contains other useful references which cannot all be cited here.

1.2 *Objectives*

This paper specifically focuses on Rayleigh damping because it is very commonly used in earthquake engineering. It is often expressed as a damping ratio ξ associated to two modal frequencies at certain times in the structural history. A first objective of this paper is to assess how the uncertainty on ξ propagates to the outcomes of interest of inelastic time history analysis (ITHA). In particular, we aim at assessing the sensitivity of the model performance outputs to ξ, and at quantifying the contribution of an uncertain ξ to the overall dispersion in the outputs. The other source of uncertainty considered is the ground motion, with record-to-record and peak acceleration variability.

When performing ITHA, Rayleigh damping not being added to solely convey intrinsic structural properties ("pure" damping) yields another objective for this paper. As stated in FEMA P692 (2009, §6.4.4), "*additional viscous damping may be used to simulate the portion of energy dissipation arising from both structural and nonstructural components that is not otherwise incorporated in the model*". For instance, in (Zona et al. 2008), Rayleigh damping is added in the nonlinear seismic analysis of steel-concrete composite frames to account for energy dissipation due to friction between steel beams and concrete slabs, which indeed is not explicitly introduced in the inelastic structural model due to a lack of quantitative information about this mechanism. Another objective is thus to investigate the sensitivity to the variable ξ of the energy absorbed by either the structural model or the additional Rayleigh damping model.

1.3 *Outline*

In the next section, we clarify the dual very nature of the structural and additional damping models and recall some basics of the state of the practice for using Rayleigh damping in ITHA. Section 3 is devoted to the description of the random variables we introduce to account for uncertainty in both the seismic loading and the Rayleigh damping model. Then, in a fourth section, the deterministic test structure used in the estimation of the effects of the uncertain variables in the ITHA outputs is presented. This is a reinforced concrete moment-resisting frame that was tested on a shaking table. Its numerical inelastic structural model is briefly presented and a deterministic analysis is run to assess the capability of this model to retrieve displacement-based performance as well as energy quantities observed during the experimental test. Then, Latin hypercube samples of the random variables are generated and Monte Carlo simulations are performed to propagate the uncertainty. Results of various uncertainty and sensitivity analyses are shown and discussed in section 5. The main results of this work are summarized in the concluding section.

2 RAYLEIGH DAMPING IN INELASTIC TIME HISTORY ANALYSIS

2.1 *Rational definition for damping*

For earthquake engineering applications, a general form of the models used to predict a set of outputs $\mathbf{b}$ from both a set of inputs $\mathbf{a}$ and a set of parameters $\boldsymbol{\theta}$ can be given as (see figure 1):

$$\mathbf{b} = \mathcal{M}(\mathbf{a}, \boldsymbol{\theta}) = \mathcal{K}(\mathbf{a}^{\mathcal{K}}, \boldsymbol{\theta}^{\mathcal{K}}) + \mathcal{D}(\mathbf{a}^{\mathcal{D}}, \boldsymbol{\theta}^{\mathcal{D}}) \tag{1}$$

where $\mathcal{K}$ represents the structural model and $\mathcal{D}$ is an additional damping model commonly used in practice to convey, at the structural level, the effects of all the energy dissipative mechanisms not otherwise explicitly accounted for in $\mathcal{K}$.

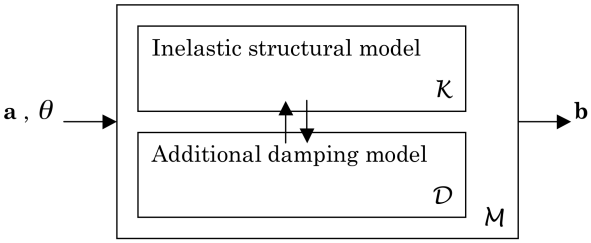

Figure 1: System for earthquake engineering applications. The model $\mathcal{M}$ allows for predicting a set of outcomes $\mathbf{b}$ from a set of inputs $\mathbf{a}$ and of parameters $\boldsymbol{\theta}$. $\mathcal{M}$ results from the interaction between structural and damping sub-models $\mathcal{K}$ and $\mathcal{D}$.

The discretized structural model $\mathcal{K}$ takes the form:

$$(\mathcal{K}) \quad \mathbf{f}^{\,kin}(\ddot{\mathbf{d}}_n) + \mathbf{f}^{\,int}(\mathbf{d}_n) = \mathbf{f}^{\,sei}(\ddot{\mathbf{u}}_n^{sei}) + \mathbf{f}^{\,sta}$$

where $\mathbf{f}^{\,kin}$, $\mathbf{f}^{\,int}$, $\mathbf{f}^{\,sei}$ and $\mathbf{f}^{\,sta}$ are the inertia, internal, seismic, and static forces vectors. $\mathbf{d}$ is the discrete displacements vector.

Adding damping to $\mathcal{K}$ defines the model $\mathcal{M}$ as:

$$(\mathcal{M}) \quad \mathbf{f}_n^{kin} + \mathbf{f}_n^{int} + \mathbf{f}_n^{dam}(?) = \mathbf{f}_n^{sei} + \mathbf{f}^{\,sta} \tag{2}$$

where $\mathbf{f}^{\,dam}$ is the additional damping force vector. In most of the practical applications, the damping is hysteretic and/or viscous, thus $? = \mathbf{d}_n$ or $? = \dot{\mathbf{d}}_n$, but it could take any other form, as long as equation (2) can be effectively resolved.

Among the models $\mathcal{K}$ and $\mathcal{D}$, only the structural model $\mathcal{K}$ can genuinely be qualified as "physical". Indeed, it is developed in consistence with the theory of continuum mechanics. However, there is no such a well-established theory which damping model $\mathcal{D}$

could be developed in. Nevertheless, equation (2) defines a relation of duality between models $\mathcal{K}$ and $\mathcal{D}$ which serves as the baseline for the following definition of a physical damping model: a model that completes the structural model for a reliable prediction of the model $\mathcal{M}$ outcomes of interest.

2.2 *Rayleigh damping model*

One now has to choose a damping model that would satisfy the rational definition above. In most of the applications in earthquake engineering, Rayleigh damping is chosen, that is, in the most general form:

$$\mathbf{f}^{dam} = \mathbf{C}(t)\dot{\mathbf{d}}(t) \text{ with } \mathbf{C}(t) = \alpha(t)\mathbf{M} + \beta(t)\mathbf{K}(t) \quad (3)$$

where $\mathbf{M}$ and $\mathbf{K}$ are the mass and stiffness matrices and (α, β) are computed according to both two modal frequencies at certain times in the structural history and a targeted damping ratio $\hat{\xi}$. Whether the initial or the tangent stiffness matrix is used and whether α and β are taken as time-dependent or not has to be decided regarding the consequences those assumptions imply (Charney 2008, among others).

Some other practical aspects of Rayleigh damping:
(i) Adding a small amount of damping, say $\hat{\xi} < 0.5\%$, is often necessary to guarantee the good convergence of the overall resolution algorithm;
(ii) Usual practice for reinforced concrete low-rise frames consists in targeting a damping ratio of about 5% for the dominant structural modes. This is larger than the 0.5% to 1.5% of "pure" damping classically observed for low-amplitude oscillations, which implies that using Rayleigh damping for representing mechanisms "not otherwise incorporated in the model" or poorly described by the structural model is common practice in ITHA.

3 RANDOM VARIABLES

3.1 *Ground motion dataset*

To account for record-to-record variability of the seismic loading, we select a dataset in the PEER ground motion database with its Web application (PGMD 2011), so that the selected ground motions are consistent with i) the likely earthquake scenarios and ii) the soil properties in the region where the design ground motion was recorded, *viz.* the Cascadia subduction zone, and iii) exhibit good match with the target design spectrum in the most important period range.

The Cascadia subduction zone is an active seismic area that has been observed for several decades (Silva et al. 1998, Wiest et al. 2007, among others) and it has been reported that three types of earthquakes are produced in this zone:
(i) *Shallow crustal earthquakes* due to surface faults in the American continental plate with magnitude M_w larger than 7.0 and hypocenter depth less than 30 km;
(ii) *Thrust interplate or interface earthquakes* generated by differential motion in the interface between the two plates. Such earthquakes happen offshore with surface hypocenter, generally with depth less than 30 km. In the Cascadia subduction zone, a large event of this kind is likely to be produced with magnitude $M_w = 8.3 \pm 0.5$;
(iii) *Intraplate or intraslab earthquakes* occur deep within the Cascadia subduction zone (depth $>$ 40 km).
For depth larger than 100 km, no seismic activity has been observed.

As far as the soil properties in this region are concerned, the geologic profile of the station where the design ground motion was recorded is detailed in table 1 (Silva et al. 1998).

Table 1: Geologic profile for the Olympic Highway Test Lab strong-motion recording site in Washington. v_s is the shear wave velocity and ρ the density.

Depth (m)	Geology	Description	v_s (m/s)	ρ (kg/m^3)
0-3	Fill	Loose sand.	165	1500
3-12	Deposits	Medium dense fine to medium sand.	220	1500
12-20	Deposits	Interbedded very stiff to hard sandy silt and very dense silty fine to medium sand.	270	1500
20-41	Deposits	(*Like just above.*)	330	1500

The PEER database is currently limited to recorded time series from shallow crustal earthquakes. The initial acceptance criteria used for the search of ground motions are as follows: moment magnitude $M_w \in [7.0, 9.0]$, Joyner-Boore distance $R_{JB} \in [0, 150]$ km, closest distance to rupture plane $R_{rup} \in [0, 150]$ km, and average shear wave velocity in the top 30 meters of the site $v_{s30} \in [0, 200]$ m/s. With these criteria, approximately 20 earthquakes were identified. To increase the number of different recoding stations, we proceeded to a second search with the range of allowed moment magnitudes extended to $M_w \in [6.0, 9.0]$ and finally selected 20 ground motions.

Equal probability is attributed to every ground motion in the dataset.

3.2 *Peak acceleration of the ground motions*

Displacement-based EDPs such as the interstory drift generally strongly depends on the horizontal peak acceleration of the ground motion. Besides, probabilistic seismic hazard often is expressed in term of PGA or spectral acceleration in a given geographical region. In other words: uncertainty in PGA is both an accessible data and expected to cause uncertainty in the EDPs. We therefore add PGA as another source of uncertainty in our analysis.

Every ground motion is first normalized to PGA = 1 g and then scaled to a value between 0.1

and 0.4. The scale factor is random and computed as:

$$\lambda_a = 0.1 + 0.05(N_a - 1) \quad \text{with} \quad N_a \sim d\mathcal{U}(1,7) \quad (4)$$

where $d\mathcal{U}(n), n \in \mathbb{N}$, is the discrete uniform probability density function.

If our objective were to perform a seismic risk analysis and not only a structural performance study, seismic hazard curves should be used here instead of a uniformly distributed scale factor. For the sake of illustration, we mention that according to the 1985 seismic zoning map of the National Building Code of Canada, ground motions with horizontal PGA between 0.16 g and 0.23 g is likely to be observed with a probability of exceedance of 10% in 50 years in the Canadian Cascadia subduction zone.

3.3 *Target damping ratio* $\hat{\xi}$

The last random variable considered is the target damping ratio $\hat{\xi}$ characterizing the amount of Rayleigh damping in the simulation (sub-model $\mathcal{D}$). This variable can both have an influence on the performance EDPs (outcomes of model $\mathcal{M}$) and on the behavior of the interrelated structural sub-model $\mathcal{K}$. The two damping ratios needed to build the Rayleigh damping matrix are taken as equal in the range $[1\%, 10\%]$ without assuming any knowledge on the actual value:

$$\hat{\xi}[\%] = 1 + \frac{9}{50}(N_\xi - 1) \quad \text{with} \quad N_\xi \sim d\mathcal{U}(1,50) \quad (5)$$

Rayleigh damping can be introduced either at the level of the whole structure or at the level of the structural elements. The second option should be retained because there is no reason to assign the same damping ratio to structural elements which only have few in common. In other words, the hypothesis of perfect spatial correlation of the damping ratios does not hold. Indeed, as already mentioned, we do not limit our analysis to the sub-model $\mathcal{D}$ solely representing "pure" damping but also as an ad hoc source of energy dissipation in addition to the energy dissipation coming from the nonlinear mechanisms in the sub-model $\mathcal{K}$. If only "pure" damping were at stake, this would not be worth considering this correlation except for composite structures composed by elements made of different materials. The analysis outcomes can be affected by this obvious correlation between damping ratios pertaining to different structural elements. As previous evidence of the potential effects of space correlations in ITHA performance outputs, one can cite the work of Stefanou and Fragiadakis (2009).

4 DETERMINISTIC NUMERICAL INELASTIC SIMULATION

4.1 *Description of the structure*

The test structure considered to estimate the effects of the selected random variables on the performance outputs of ITHA is depicted in figure 2. It was designed at a reduced scale of $1/2$ according to the provisions of the National Building Code of Canada and of the Canadian concrete standard. The structure was assumed to have a nominal ductility, that is a design base shear computed with a reduction factor $R = 2$. Four concrete blocks were used to simulate concentrated gravity loads in every beam span; they were designed so that their center of gravity coincide with the center of gravity of the supporting beam. These latter additional masses induced service cracks. The total weight of the frame was 95 kN, its fundamental period $T_1 = 0.36$ s was measured preliminary to the seismic excitation. Mode 1 is preponderant in the sense that it accounts for 91% of the total mass. The detailed presentation of the design assumptions and parameters can be found in (Filiatrault et al. 1998).

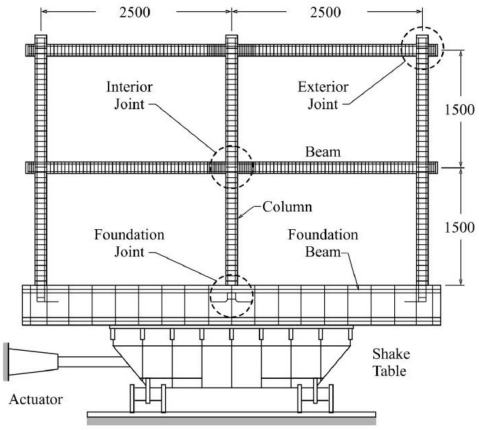

Figure 2: RC frame structure tested on the shaking table at École Polytechnique in Montreal. Dimensions are in [mm].

The N04W component of the accelerogram recorded in Olympia, Washington on April 13, 1949 was selected for the test program and scaled to a peak ground acceleration PGA = 0.21 g. The feedback record of the acceleration measured on the shaking table during the test is shown in figure 3 along with the corresponding elastic response spectrum with 5% viscous damping ratio.

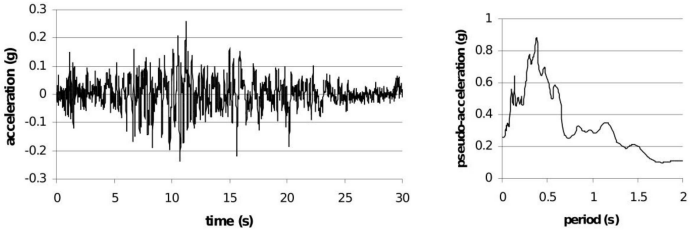

Figure 3: Acceleration time history recorded on the shaking table during the test and corresponding elastic response spectrum with a critical viscous damping ratio of 5%.

4.2 *Structural model* $\mathcal{K}$

Fiber beam/column elements implemented in the framework of a displacement-based finite element

method with Euler-Bernoulli kinematics are used to model the response of the structural elements of the frame. The finite element mesh of the RC frame is shown in figure 4. The structure is assumed fixed at its base. Rigid end zones are added to model the beam-to-column connections and rebar slip in surrounding concrete is not represented. These later hypotheses are questionable because the beam-to-column connections exhibited inelastic behavior during the test.

The uniaxial constitutive laws used to model steel and both confined and unconfined concrete fibers are also shown in figure 4. The inelastic model used to represent the salient features of the materials cyclic behavior has been developed in the framework of thermodynamics with internal variables and is presented in (Jehel et al. 2010). The set of parameters has been identified to fit experimental monotonic curves. From the computational point of view, because hardening and softening laws are modeled as linear, there is no need for local iteration when the internal variables – the memory of the materials – are updated, except for transitions between hardening and softening regimes, which makes the resolution procedure robust and efficient.

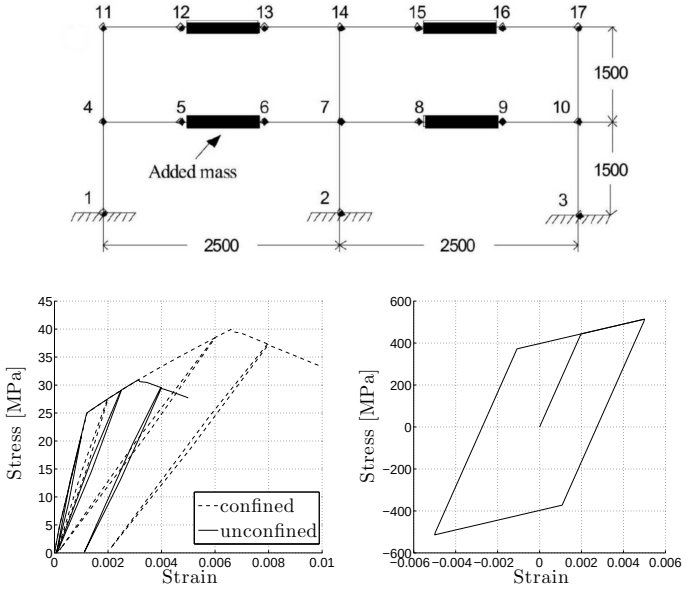

Figure 4: Finite element mesh (dimensions in [mm]) and material constitutive laws for the inelastic structural modeling. [bottom left] Confined and unconfined concrete behavior laws. [bottom right] Steel constitutive law.

The loading time history consists in two phases: i) static dead load is first applied step by step and then kept constant; ii) the seismic loading is applied. A first validation check of the inelastic structural model is carried out by simulating a free vibration test. Before dead load is applied, the elastic fundamental period of the structure is computed as $T_1^{ela} = 0.28$ s; then, due to the inelastic behavior of the structure, the elongated period is evaluated as $T_1^{ini} = 0.36$ s when dead load is completely applied. Both T_1^{ela} and T_1^{ini} coincide with the experimental values.

4.3 *Rayleigh damping model $\mathcal{D}$*

For all the ITHA that will be run in the following, the Rayleigh damping model is build with tangent stiffness matrix and designed according to the procedure presented in (Jehel et al. 2013) so that the effective modal damping ratios remains as close as possible to a targeted damping ratio $\hat{\xi}$ while structure deteriorates.

4.4 *Energy quantities*

The following energy quantities will be considered:
Hysteretic energy: $E_H = \int_0^T \int_\Omega \boldsymbol{\sigma} : \dot{\boldsymbol{\epsilon}} \, d\Omega \, dt$;
Damping energy: $E_D = \int_0^T \mathbf{f}^{\,dam} \cdot \dot{\mathbf{u}} \, dt$;
Total energy: $E_{tot} = E_H + E_D$.

4.5 *Numerical vs. experimental results*

For this modeling of the experimental test, a targeted damping ratio $\hat{\xi} = 2\%$ is used. For this simulation as well as for all the simulations in the next section, Newmark β-method with $\gamma = 0.5$ and $\beta = 0.25$ with a time step of 5.10^{-3} s is employed. Computed displacement-based performance outcomes and energy quantities are summarized and confronted to experimental data in table 2 and figure 5.

Table 2: Experimental and numerical results. MRD is the maximum roof displacement, $MISDR$ the maximum inter-story drift ratio, and E_{tot} the total energy absorbed by the system.

	MRD (mm)	MISDR (%)	E_{tot} (N.m)
Exp.	48.9	2.0	2850
Num.	43.3	1.7	2822

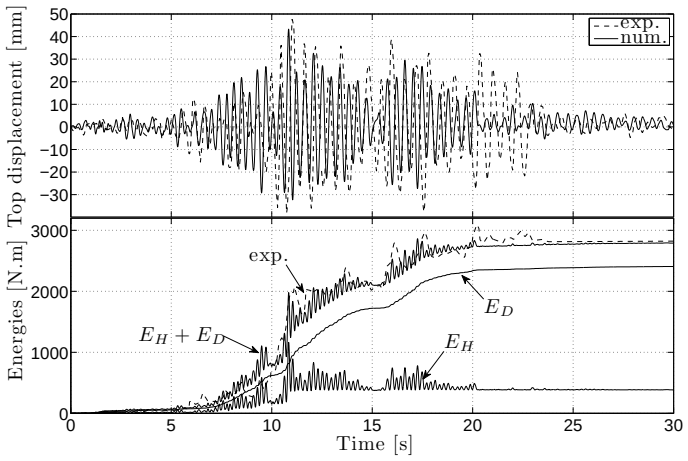

Figure 5: Comparison of experimental and numerical results. E_H is the energy absorbed by the sub-model $\mathcal{K}$, E_D is the energy absorbed by the additional Rayleigh damping sub-model $\mathcal{D}$ designed with targeted damping ratio is $\hat{\xi} = 2\%$.

5 UNCERTAINTY AND SENSITIVITY ANALYSES

The structural model will remain unchanged all along the following uncertainty and sensitivity analyses and,

consequently, all the probabilistic quantities hereafter discussed have to be understood as conditional to the model $\mathcal{K}$.

5.1 *Uncertainty analysis*

Two Latin hypercube samples $\mathcal{S}_1$ and $\mathcal{S}_2$ of size $N = 1000$ of the random variables are generated from the probability spaces $\mathcal{P}_1$ and $\mathcal{P}_2$ (McKay et al. 1979). The random parameter for ground motion record-to-record variability is denoted as GM#. The events in $\mathcal{P}_1$, resp. in $\mathcal{P}_2$, are the triplets (GM#, PGA, $\hat{\xi}$), resp. the (N^e+2)-tuple (GM#, PGA, $[\hat{\xi}^e, e = 1, .., N^e]$) where N^e is the number of elements in the finite element mesh of the modeled structure. The random variables are considered as independent, although attenuation laws could for instance provide indication about how the distance to rupture plane – the GM#, in turn – is correlated to PGA. Also, $\mathcal{P}_1$ describes perfectly spatially correlated damping ratios, whereas $\mathcal{P}_2$ accounts for spatially independent damping ratios.

Uncertainty is propagated to the model outputs with Monte Carlo simulations. The uncertainty analysis of the maximum interstory drift ratio ($MISDR$) is shown in figures 6 for sample $\mathcal{S}_1$ and in figures 7 for sample $\mathcal{S}_2$ (figures on next page). The distributions are slightly different and, in the following, only the results obtained with sample $\mathcal{S}_1$ will be discussed.

5.2 $MISDR$ *sensitivity*

From figure 8 (figure on last page), the following trends can be observed: i) The absolute variability increases with PGA; ii) The variability in $MISDR$ due to the Rayleigh damping ratio is generally much less significant than the variability due to PGA, except for some records (*e.g.* GM# = 8 or GM# = 17).

Figures 9, 10 and 11 also provide insight into the sensitivity of $MISDR$ to the three random variables considered in this study. The clear linear correlation between $MISDR$ and PGA, which is usually assessed in the preliminary study to structural vulnerability analysis, is also observed here in figure 9. Indeed, the mean of $MISDR$ linearly increases with PGA, and the relatively small COV($MISDR$|PGA) – compared to the overall COV observed in figure 6 – provides good confidence in the computed means. COV($MISDR$|PGA) being approximately half COV($MISDR$) also shows that PGA is an important contributor to the overall uncertainty in $MISDR$. Figures 10 and 11 show that GM# and $\hat{\xi}$ less importantly contribute to the uncertainty in $MISDR$. Same conclusions are drawn in the studies of Porter et al. (2002) and Lee and Mosalam (2005).

Focussing now on figure 11, one may jump to the following intuitive conclusion when looking at the mean E($MISDR|\hat{\xi}$): the larger the Rayleigh damping ratio, the smaller the $MISDR$. Although actually a general trend, this is however to be taken with caution for two reasons: i) the number of data computed for a given $\hat{\xi}$ is around 20 only, and ii) the large dispersion of the data (COV($MISDR|\hat{\xi}$) is large) entails small confidence in the mean.

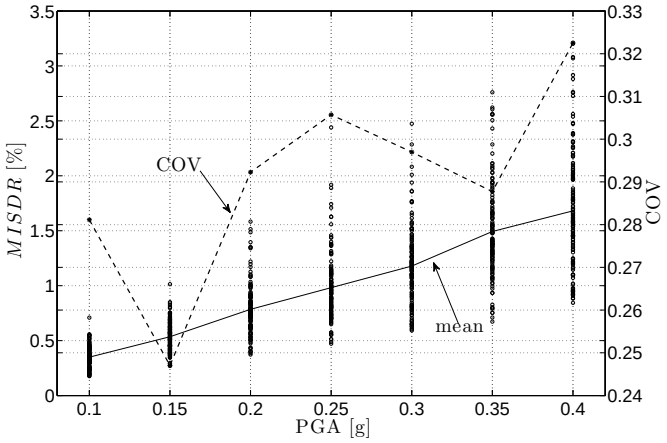

Figure 9: $MISDR$ w.r.t. the 7 PGA levels considered in the analysis. Scatter is due to the variability in GM and $\hat{\xi}$.

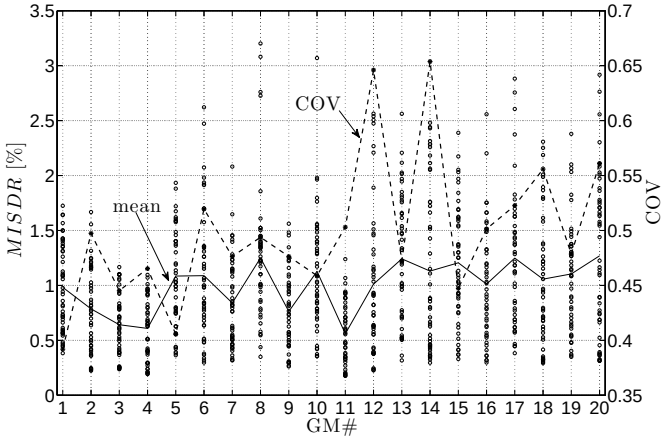

Figure 10: $MISDR$ w.r.t. the 20 ground motion records used in the analysis. Scatter is due to the variability in PGA and $\hat{\xi}$.

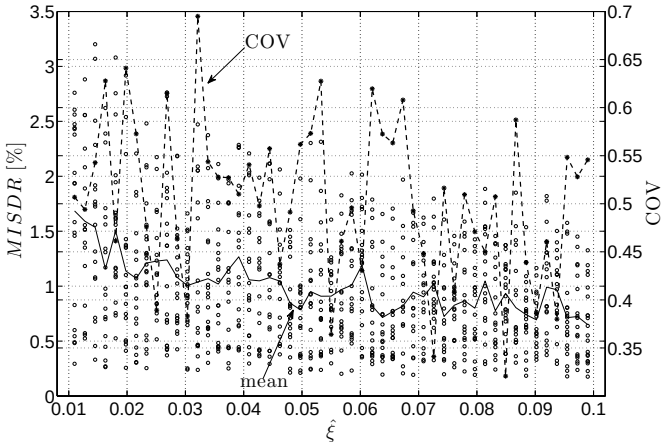

Figure 11: $MISDR$ w.r.t. increasing Rayleigh damping ratio. Scatter is due to the variability in GM and PGA.

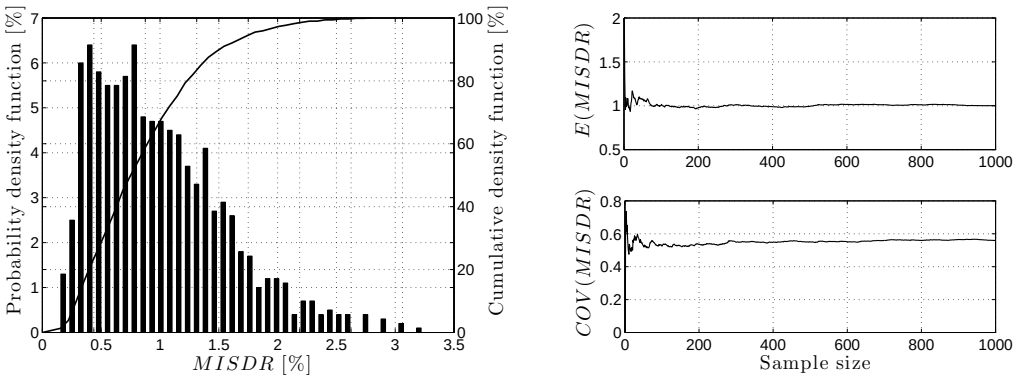

Figure 6: Distribution of the maximum interstory drift, as well as its mean and COV convergence assessment for sample $\mathcal{S}_1$.

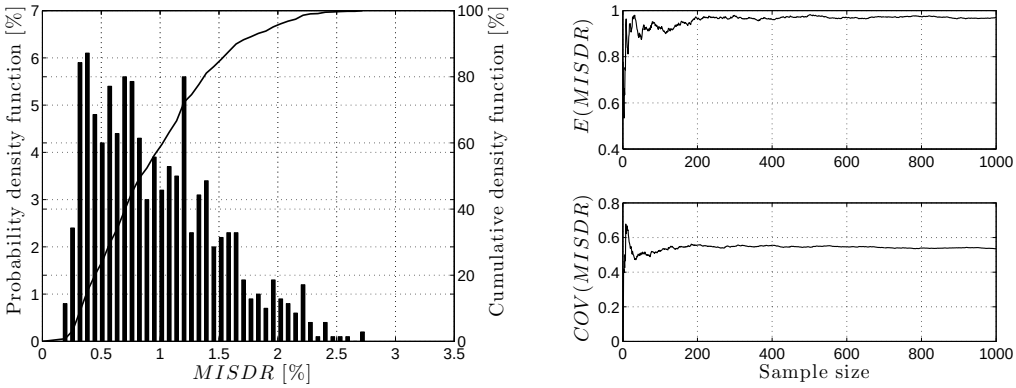

Figure 7: Distribution of the maximum interstory drift, as well as its mean and COV convergence assessment for sample $\mathcal{S}_2$.

5.3 *Energy sensitivity*

The observation of energy quantities is used to provide insight into the sensitivity of the interrelation between models $\mathcal{K}$ and $\mathcal{D}$ to the random variables. The mean values E($E_{tot}|\hat{\xi}$) in figure 12 shows that the total amount of energy absorbed by the model $\mathcal{M}$ is weakly correlated to the Rayleigh damping ratio (E(E_{tot}) = 2408 N.m for sample $\mathcal{S}_1$ and to 2364 N.m for $\mathcal{S}_2$). This again has to be taken with caution because the means are computed with only 20 values that, besides, exhibit large scatter (COV($E_{tot}|\hat{\xi}$) is to be compared to the overall COV(E_{tot}) which is equal to 0.98 for sample $\mathcal{S}_1$ and to 1.01 for $\mathcal{S}_2$, which also shows that the main contribution to the overall variability of E_{tot} comes from the ground motion). Nevertheless, the small influence of $\hat{\xi}$ on E_{tot} is in accordance with the observations of Léger and Dussault (1992). With much less scatter (approximately 5% $<$ COV($DER|\hat{\xi}$) $<$ 25%), figure 13 shows that the share of the total energy E_{tot} absorbed by model $\mathcal{D}$ tends to increase with $\hat{\xi}$.

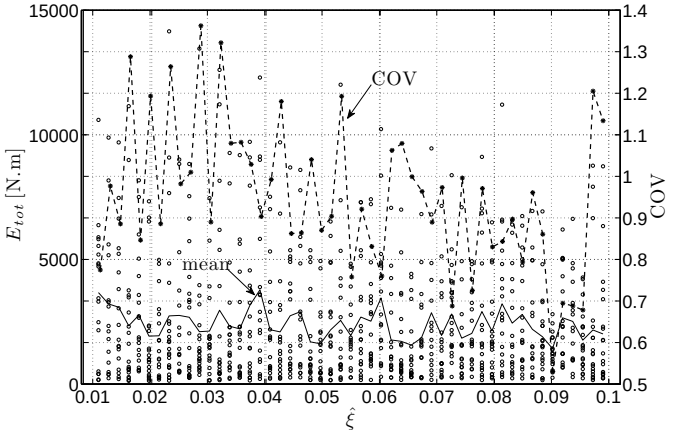

Figure 12: Total energy absorbed by the model $\mathcal{M}$ throughout ITHA w.r.t. increasing Rayleigh damping ratio. Scatter is due to the variability in GM and PGA.

6 CONCLUSIONS

In this paper, the impact of random variables on the performance outcomes of seismic inelastic time history analyses of a reinforced concrete moment-resisting frame is investigated. The random variables considered describe uncertainty in the seismic ground motion and in the Rayleigh damping model added in the simulations to account for the energy dissipative mechanisms not otherwise represented in the structural model. Latin hypercube samples of the uncorrelated random variables are generated and Monte Carlo simulations are run to propagate the uncertainty. Effects of spatial correlation of the Rayleigh damping parameters are briefly investigated. In the case of perfect correlation between the damping properties, the following observations have been made: i) the variability in the maximum interstory drift ratio ($MISDR$) is mainly due to the variability in the peak acceleration of the ground motion; ii) however, for a few ground motion records, the Rayleigh damping ra-

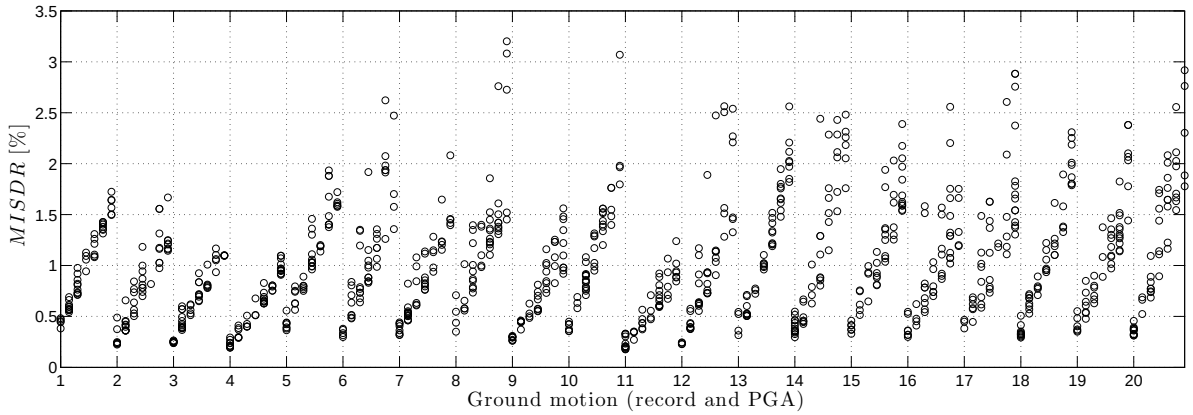

Figure 8: $MISDR$ w.r.t. the 140 ground motions considered in the analysis. The figure can be read as follows: GM# is indicated on the x-axis; between two successive GM#, a right shift indicates a PGA increase of 0.05 g; then, the scatter following any vertical line is due to the sole variability in $\hat{\xi}$.

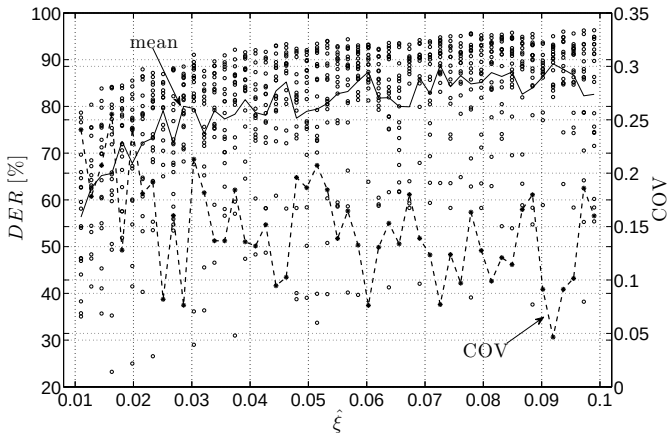

Figure 13: Ratio of the energy absorbed by the Rayleigh damping model $\mathcal{D}$ throughout ITHA w.r.t. increasing Rayleigh damping ratio. Scatter is due to the variability in GM and PGA. Balancing ratio of the energy absorbed by the structural model $\mathcal{K}$ throughout ITHA is $HER = 100\%\text{-}DER$.

tio can be a very important contributor to the variability in $MISDR$; iii) the correlation between the total amount of energy absorbed by the model and the Rayleigh damping ratio tends to be weak; iv) the share of the total energy absorbed by the damping model tends to increase with the Rayleigh damping ratio.

ACKNOWLEDGMENTS

This research is supported by a Marie Curie International Outgoing Fellowship within the 7th European Community Framework Programme (proposal No. 275928). I thank Prof. Deodatis for valuable discussions during the preparation of this work.

REFERENCES

Charney, F. A. (2008). Unintended consequences of modeling damping in structures. *J Struct Eng-ASCE 134*(4), 581–592.

FEMA P692 (2009, June). Quantification of building seismic performance factors. Technical Report FEMA P695.

Filiatrault, A., E. Lachapelle, & P. Lamontagne (1998). Seismic performance of ductile and nominally ductile reinforced concrete moment resisting frames. I. Experimental study. *Can J Civil Eng 25*, 331–341.

Hwang, H. H. & J.-R. Huo (1994). Generation of hazard-consistent fragility curves. *Soil Dyn Earthq Eng 13*(5), 345–354.

Jehel, P., L. Davenne, A. Ibrahimbegovic, & P. Léger (2010). Towards robust viscoelastic-plastic-damage material model with different hardenings / softenings capable of representing salient phenomena in seismic loading applications. *Computers and Concrete 7*(4), 365–386.

Jehel, P., P. Léger, & A. Ibrahimbegovic (2013). Initial vs. tangent stiffness-based Rayleigh damping in inelastic time history seismic analyses. *Submitted*.

Lee, T.-H. & K. M. Mosalam (2005). Seismic demand sensitivity of reinforced concrete shear-wall building using FOSM method. *Earthquake Engng Struct. Dyn. 34*, 1719–1736.

Léger, P. & S. Dussault (1992). Seismic-Energy Dissipation in MDOF Structures. *J Struct Eng-ASCE 118*(6), 1251–1267.

Liel, A. B., C. B. Haselton, G. G. Deierlein, & J. W. Baker (2009). Incorporating modeling uncertainties in the assessment of seismic collapse risk of buildings. *Struct Saf 31*, 197–211.

McKay, M. D., R. J. Beckman, & W. J. Conover (1979). A comparison of three methods for selecting values on input variables in the analysis of output from a computer code. *Technometrics 21*(2), 239–245.

PGMD (2011, November). Users manual for the PEER ground motion database Web application. Technical report, Pacific Earthquake Engineering Research Center.

Porter, K. A., J. L. Beck, & R. V. Shaikhutdinov (2002). Sensitivity of building loss estimates to major uncertain variables. *Earthquake Spectra 18*(4), 719–743.

Silva, W. J., I. G. Wong, & R. B. Darragh (1998). *Assessing earthquake hazards and reducing risk in the Pacific Northwest*, Volume 2, Chapter Engineering characterization of earthquake strong motions in the Pacific Northwest, pp. 313–324. Washington: United States Government Printing Office.

Stefanou, G. & M. Fragiadakis (2009). Nonlinear dynamic analysis of frames with stochastic non-gaussian material properties. *Eng Struct 31*, 1841–1850.

Tantala, M. W., G. J. P. Nordenson, G. Deodatis, & K. Jacob (2008). Earthquake loss estimation for the New York City Metropolitan Region. *Soil Dyn Earthq Eng 28*, 812–835.

Vamvatsikos, D. & M. Fragiadakis (2010). Incremental dynamic analysis for estimating seismic performance sensitivity and uncertainty. *Earthquake Engng Struct. Dyn. 39*, 141–163.

Wiest, K. R., D. I. Doser, A. A. Velasco, & J. Zollweg (2007). Source investigation and comparison of the 1939, 1946, 1949 and 1965 earthquakes, Cascadia subduction zone, Western Washington. *Pure Appl Geophys 164*, 1905–1919.

Zona, A., M. Barbato, & J. P. Conte (2008). Nonlinear seismic response analysis of steel–concrete composite frames. *J Struct Eng-ASCE 134*(6), 986–997.